SIMPLE AND FAST GRADIENT-BASED IMPEDANCE INVERSION USING TOTAL VARIATION REGULARIZATION

DANIEL O. PÉREZ[1,2] AND DANILO R. VELIS[1]

[1] Facultad de Ciencias Astronómicas y Geofísicas, Universidad Nacional de La Plata, and CONICET; Argentina. dperez@fcaglp.unlp.edu.ar
[2] YPF Tecnología S.A., Av. Del Petroleo s/n, Berisso, Argentina.
velis@fcaglp.unlp.edu.ar

(Received October 24, 2017; revised version accepted July 20, 2018)

ABSTRACT

Pérez, D.O. and Velis, D.R., 2018. Simple and fast gradient-based impedance inversion using total variation regularization. *Journal of Seismis Exploration*, 27: 473-486.

We present an algorithm to estimate blocky images of the subsurface acoustic impedance (AI) from poststack seismic data. We regularize the resulting inverse problem, which is inherently ill-posed and non-unique, by means of the total variation semi-norm (TV). This allows us promote stable and blocky solutions which are, by virtue of the capability of TV to handle edges properly, adequate to model layered earth models with sharp contrasts. The use of the TV leads to a convex objective function easily minimized using a gradient-based algorithm that requires, in contrast to other AI inversion methods based on TV regularization, simple matrix-vector multiplications and no direct matrix inversion. The latter makes the algorithm numerically stable, easy to apply, and economic in terms of computational cost. Tests on synthetic and field data show that the proposed method, contrarily to conventional l_2- or l_1-norm regularized solutions is able to provide blocky AI images that preserve the subsurface layered structure with good lateral continuity from noisy observations.

KEY WORDS: acoustic impedance, inversion, poststack, total variation, blocky, FISTA.

0963-0651/18/$5.00

INTRODUCTION

The inversion of poststack seismic data to estimate AI images is a common technique used to obtain information about the structure of the subsurface. It allows to establish relations between the recorded seismic data and the geology (Oldenburg et al., 1983). Inverse problems are usually solved by minimizing a cost function that measures the differences between the observed and the modeled data (Tarantola, 2005). Unfortunately, the solutions of most geophysical inverse problems are inherently non-unique, for there exists several solutions that honor the data equally well. Furthermore, seismic inversion is an ill-posed problem, meaning that little amounts of noise in the observed data lead to large errors in the estimated solutions. For the sake of stabilization, and to avoid meaningless solutions, an appropriate regularization must be used during the inversion process. A well-chosen regularization can also impart desirable characteristics to the estimated solution, as sparseness or blockiness (Ulrych and Sacchi, 2005). In addition, as consequence of the band-limited nature of the seismic data, there is a lack of low frequency information that must be incorporated into the inversion process to properly constrain the estimated AI solutions. The inversion strategy must overcome the aforementioned drawbacks in a computationally efficient way, as the amount of seismic data to process is usually large.

The AI inversion can be separated into reflectivity domain inversion and data domain inversion (Gholami, 2016). In the former the reflectivity is estimated from the seismic data via deconvolution, and then the AI is derived from the reflectivity by recursive integration. In the later the AI is directly estimated from the seismic data. Also, depending on if the source wavelet is known a priori or it is estimated during the inversion process, the inversion can be separated into non-blind and blind. In this sense, several authors have developed AI inversion techniques with very interesting results (Oldenburg et al., 1983; Cooke and Schneider, 1983, e.g.). In the context of blocky AI inversion, Velis (2005, 2008) proposed to use either a constrained inversion strategy based on Gibb's sampling, or the global optimization algorithm known as very fast simulated annealing for the non-blind AI inversion in the data and reflectivity domains, respectively. Also, in the reflectivity domain, Gholami and Sacchi (2013) derived an AI inversion algorithm based on the split Bregman iteration method (Goldstein and Osher, 2009). Based on the same strategy, Gholami (2015, 2016) and Li and Peng (2017) developed various techniques to perform both non-blind and blind AI inversions in the data domain.

In this work we propose an alternative algorithm for the non-blind multichannel AI inversion in the data domain. It relies on the TV semi-norm (Rudin et al., 1992; Chambolle, 2004) regularization to promote blocky solutions of the AI, which leads to a convex cost function that can be minimized using an efficient iterative gradient-based algorithm that requires

no matrix inversion (Beck and Teboulle, 2009a). It is worth mentioning that blocky solutions are desirable because they lead to sharply resolved discontinuities that overcome the band-limitation of classical l_2-norm solutions. Based on impedance well logs information, one may argue that the real structure of the subsurface is continuous rather than layered (Cooke and Schneider, 1983). Nevertheless, it is known from well log data studies that the amplitudes of the reflection coefficients associated with the interfaces follow a non-Gaussian distribution (Walden and Hosken, 1986; Velis, 2003). This fact indicates that the main lithological units can be represented by layers with certain properties.

Many blocky AI inversion methods, including the aforementioned ones, assume the validity of the convolutional model and rely on the minimization of some regularized cost function. As usual, the overall impact of the regularizations is controlled by trade-off parameters which must be chosen to make optimal use of the data observations. Given a regularized cost function, it is the algorithm used to carry out the minimization what distinguishes one method from the other. Ultimately, all AI solutions are very similar. Depending of the problem at hand, slightly improved solutions can be obtained using extra regularization terms or a debiasing step (Figueiredo et al., 2007), but at the expense of increasing the computational cost. For example, Li and Peng (2017) obtained blocky AI solutions minimizing a combination of l_1 and l_2-norms. Although successful, this approach leads to a complex mathematical scheme in which a system of equations must be solved in each step of an iterative process. This is to the detriment of numerical stability and computational efficiency, especially if the used solver requires matrix inversions. The method proposed in this paper uses the TV regularization and only requires matrix-vector multiplications, making it numerically stable, versatile, easy to apply and computationally efficient. Regarding other TV-related methods, authors such as Liu and Yin (2015), Li and Peng (2017), Wang and Gao (2017) and Wang et al. (2017) minimize the regularized cost functions by means of a split Bregman iteration scheme. Although this strategy leads to computationally efficient algorithms, the solutions often depend on several trade-off parameters which must be chosen appropriately. In contraposition, the strategy proposed in this work only depends on a single trade-off parameter easily tuned by means of the discrepancy principle and the Pareto or L-curve. This implies a major advantage, especially when working with field data, as the trade-off parameters usually depend on the signal-to-noise ratio of the data at hand. Gholami (2015, 2016) developed a TV-related AI inversion strategy, also based in the split Bregman iteration, in which the discrete cosine transform (DCT) was used to improve the efficiency of the process. Although the algorithm is very efficient, it depends on three trade-off parameters that must be calibrated beforehand to correctly estimate blocky AI solutions. One of these parameters is associated with the low-frequency trend, which is incorporated into the iterative process as a constraint. Differently, we found out that the low-frequency trend can be

naturally incorporated into the inversion as the initial solution of the iterative process, thus avoiding the use of a difficult-to-tune trade-off parameter. Also, the proposed algorithm is simple from a mathematical and computational point of view. This makes it versatile and easy to apply in other seismic inversion problems (e.g., inversion of prestack seismic data).

This work is organized as follows. First, we explain the proposed method, we set up the necessary hypothesis and define all relevant equations. In addition, we provide a step-by-step description of the inversion algorithm. Next, we test the method on 2D synthetic poststack seismic data from the Marmousi2 model and analyze the corresponding results. Then, we test the algorithm using a 2D field data set. Also, we compare the estimated solutions with those obtained using the classical l2-norm smooth regularization and the l_1-norm sparsity-promoting regularization. Finally, the obtained results are summarized in the conclusions.

THEORY

Given a layered AI model represented by the matrix **Z** of dimension m x n, a source wavelet **w**, and assuming the validity of the convolutional model, the noisy seismic section can be expressed as

$$\mathbf{S} = \mathbf{WDX} + \mathbf{N} \quad , \tag{1}$$

with

$$\mathbf{X} = (1/2)\log(\mathbf{Z}) \quad , \tag{2}$$

where **D** is the first order difference matrix, **W** is the convolution matrix associated with the source wavelet **w**, and **N** is the additive noise term. Eq. (2) relies in the hypothesis that the contrasts of the AI across the boundaries of the layers are small compared to their absolute values. This assumption allows us to estimate the AI through a linear inverse problem (Cooke and Schneider, 1983).

Assuming that **N** contains uncorrelated Gaussian noise, the inversion is carried out minimizing the following cost function:

$$J(\mathrm{X}) = (1/\sigma^2)\,\|\mathbf{AX} - \mathbf{S}\|_2 + \mu TV(\mathbf{X}) \quad , \tag{3}$$

where σ^2 is the noise variance, μ is a trade-off parameter, $\mathbf{A} = \mathbf{WD}$ and

$$TV(\mathbf{X}) = \sum_{i=1}^{m-1} \sum_{j=1}^{n-1} \sqrt{(x_{i,j} - x_{i+1,j})^2 + (x_{i,j} - x_{i,j+1})^2} \quad , \tag{4}$$

is the isotropic TV semi-norm (Rudin, 1987).

The cost function $J(\mathbf{X})$ is composed of two terms, each one imposing a different constraint on $\mathbf{X}$. The first term represents the misfit between the modeled and the observed data. Its minimization will ensure that the estimated solution honors the observed data, a constraint that must be satisfied. On the other hand, the second term represents the regularization term. Its minimization will impart desirable characteristics to the estimated solutions. The overall impact of the regularization is controlled by the trade-off parameter μ. The TV is a regularization approach capable of handling edges properly. As the AI model is related to the lithology, the TV seems to be an adequate choice for layered earth models with sharp contrasts between adjacent layers. As we will show in the numerical examples this norm will impose sharpness and appropriate amplitude constraints for the estimated image $\mathbf{X}$, and thus for $\mathbf{Z}$.

The described inversion problem is viewed as the combination of a deconvolution problem and a TV denoising problem. The inherent large scales of the problems to be solved require the use of fast and simple numerical methods. For this reason, we minimize eq. (3) by means of the iterative gradient-based algorithm proposed by Beck and Teboulle (2009a). The algorithm is composed of two nested iterative processes. The outer process, detailed in Algorithm 1, performs the deconvolution of the traces and is based on the Fast Iterative Shrinkage-thresholding Algorithm (FISTA) developed by Beck and Teboulle (2009b), an algorithm that requires no matrix inversions. The inner iterative process, invoked in line 4 of Algorithm 1, is detailed in Algorithm 2 and performs the TV denoising of the deconvolved image. The TV denoising problem does not lead to a closed-form expression, then it is necessary to rely on an iterative algorithm. To this end we use the dual TV denoising iterative algorithm developed by Chambolle (2004). Like FISTA, this globally convergent TV denoising algorithm does not require any matrix inversion neither. Although the dual TV denoising algorithm seems to be appropriate in the current context, other methods can be used without loss of generality. We stress the fact that the resulting algorithm that we propose to minimize the cost function $J(\mathbf{X})$ only requires matrix-vector multiplications, making it numerically stable, versatile, easy to apply and economic in computational terms.

Due to the band-limited nature of the seismic data, it is not possible to recover the low-frequency trend $\mathbf{T}$ of $\mathbf{X}$ (and thus of $\mathbf{Z}$) during the inversion process. The low-frequency trend information must be obtained a priori from other sources (e.g. stacking velocities or well logs), and then incorporated into the inversion process by means of appropriate constraints. In this case, as indicated in the line 2 of Algorithm 1, we incorporate this information using $\mathbf{T}$ as the initial solution of the iterative process.

The Lipschitz constant of $\nabla\|\mathbf{AX}-\mathbf{S}\|^2$ required in the line 1 of Algorithm 1, is given by $L = 2\lambda_m(\mathbf{A}^T\mathbf{A})$ (Palomar and Eldar, 2010; Gramfort et al., 2013), where $\lambda_m(\cdot)$ denotes the maximum eigenvalue of its argument. In practice, we obtain the maximum eigenvalue using the power iteration method (Larson and Edwards, 1999, e.g.).

Algorithm 1 Deconvolution

input: $\mathbf{A}, \mathbf{S}, \mathbf{T}, \mu$

output: estimated AI image $\mathbf{Z}$

1: Set L as the Lipschitz constant of $\nabla\|\mathbf{AX}-\mathbf{S}\|^2$
2: set $\mathbf{X_0} = \mathbf{Y_1} = \mathbf{T}$ and $k = t_1 = 1$
3: **loop**
4: $\quad\mathbf{W}_k = \text{TV-denoising}\left(\mathbf{Y}_k - (2/L)\mathbf{A}^T(\mathbf{AY}_k - \mathbf{S}), 2\mu/L\right)$
5: $\quad\mathbf{X}_k = \text{argmin}\left(J(\mathbf{U}) \mid \mathbf{U} = \mathbf{W_k} \quad \text{or} \quad \mathbf{U} = \mathbf{X_{k-1}}\right)$
6: $\quad t_{k+1} = (1+\sqrt{1+4t_k^2})/2$
7: $\quad\mathbf{Y}_{k+1} = \mathbf{X}_k + (t_k/t_{k+1})(\mathbf{W}_k - \mathbf{X}_k) + ((t_k-1)/t_{k+1})(\mathbf{X}_k - \mathbf{X}_{k-1})$
8: $\quad$check convergence or stopping condition
9: $\quad$k=k+1
10: **end loop**
11: $\mathbf{Z} = \exp(2\mathbf{X}_k)$

Algorithm 2 TV denoising

input: $\mathbf{B}, \alpha$

output: denoised image $\mathbf{B}^*$

1: set $\{\mathbf{R}_1, \mathbf{S}_1\} = \{\mathbf{P}_1, \mathbf{Q}_1\} = \{\mathbf{0}_{(m-1)\times n}, \mathbf{0}_{(m)\times(n-1)}\}$
2: set $k = t_1 = 1$
3: **loop**
4: $\quad\{\mathbf{P}_k, \mathbf{Q}_k\} = \mathcal{P}\left(\{\mathbf{R}_k, \mathbf{S}_k\} + (1/8\alpha)\mathcal{L}^T(\mathbf{B} - \alpha\mathcal{L}(\mathbf{R}_k, \mathbf{S}_k))\right)$
5: $\quad\{\mathbf{R}_k, \mathbf{S}_k\} = \{\mathbf{P}_k, \mathbf{Q}_k\} + ((t_k-1)/t_{k+1})\{\mathbf{P}_k - \mathbf{P}_{k-1}, \mathbf{Q}_k - \mathbf{Q}_{k-1}\}$
6: $\quad t_{k+1} = (1+\sqrt{1+4t_k^2})/2$
7: $\quad$check convergence or stopping condition
8: $\quad k = k+1$
9: **end loop**
10: $\mathbf{B}^* = \mathbf{B} - \alpha\mathcal{L}(\mathbf{P}_k, \mathbf{Q}_k)$

where:

$$\mathcal{L}(\mathbf{F},\mathbf{G}) = \mathbf{H} \mid h_{i,j} = f_{i,j} - f_{i-1,j} + g_{i,j} - g_{i,j-1},$$

$$\mathcal{L}^T(\mathbf{H}) = \{\mathbf{F},\mathbf{G}\} \mid f_{i,j} = h_{i,j} - h_{i+1,j} \quad \text{and} \quad g_{i,j} = h_{i,j} - h_{i,j+1},$$

$$\mathcal{P}(\mathbf{F},\mathbf{G}) = \{\mathbf{H},\mathbf{K}\} \mid h_{i,j} = \frac{f_{i,j}}{\max\left(1, \sqrt{f_{i,j}^2 + g_{i,j}^2}\right)} \quad \text{and} \quad k_{i,j} = \frac{g_{i,j}}{\max\left(1, \sqrt{f_{i,j}^2 + g_{i,j}^2}\right)}$$

Another important practical issue to take into account is the stopping condition of the iterative process (line 8 of Algorithm 1). Ideally, the process should stop when the misfit is equal to the noise level. Unfortunately, depending on the selected trade-off parameter μ, the misfit often shows an asymptotic behavior towards the noise level and convergence is not achieved in a acceptable number of iterations. To overcome this problem we decided to stop the iterative process whenever the cost function does not show a significant variation for a given number of iterations.

EXAMPLES

Synthetic data example

In this example we test the proposed algorithm on 2D synthetic data generated from the Marmousi2 elastic model (Martin et al., 2006). Figs. 1a to 1d shows the AI of the model, the low-frequency trend obtained from smoothing the AI using a low-pass filter, and the corresponding noise-free and noisy seismic sections. For the sake of clarity, Figs. 1b and 1d shows one of every ten traces only. The data was generated using eqs. (1) and (2) with a sampling interval of 4 ms and a Ricker wavelet of central frequency f_0 = 30 Hz. We added uncorrelated band-limited Gaussian noise with $\sigma = max(|\mathbf{S}|)/10$ (i.e. S/N = 10).

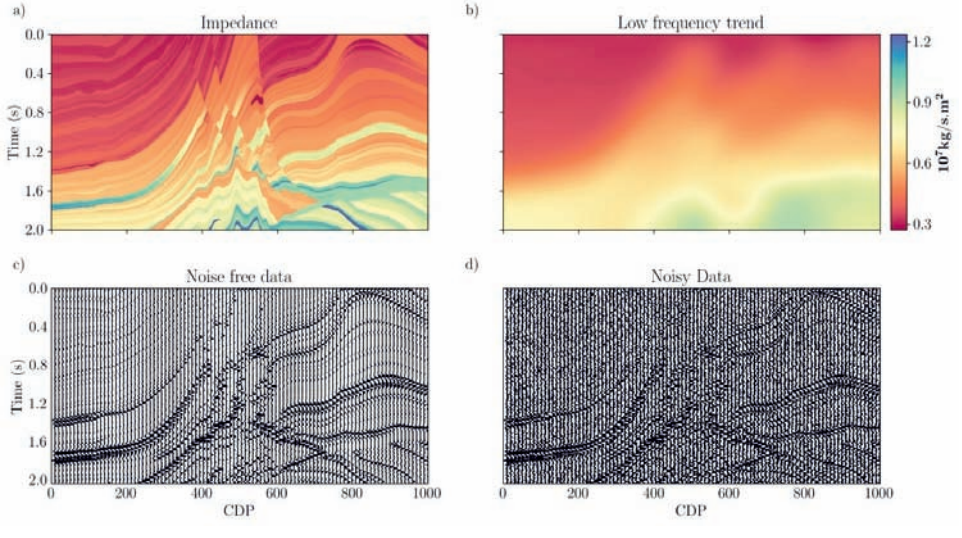

Fig. 1. a) Actual AI model generated from the Marmousi2 elastic model, b) noise-free seismic section generated from the AI model using a Ricker wavelet with f_0 = 30 Hz, c) low-frequency trend obtained from the AI model using a low-pass filter and d) noisy seismic section with S/N=10.

To apply the proposed inversion algorithm to the dataset we first need to estimate the trade-off parameter μ. In general, the selection of this parameter depends on the noise level of the data at hand. If μ is too large the regularization term in eq. (3) will be predominant over the misfit term, leading to solutions that might not honor the observed data. Contrarily, if μ is too small the noisy data might be overfit and the solutions might be too smooth. It is important to note that the trade-off parameter is not unique, for there might exist a range of μ values for which the corresponding solutions honor the observed seismic data equally well. Often, the selection of a particular value is based on the analysis of the solutions and personal judgment, especially when the data noise level is unknown (Farquharson and Oldenburg, 2004). Even so, there are various methods reported in the literature that can be used as guide to choose a value of μ. For instance, one can adopt the so-called L-curve criterion, the discrepancy principle, the generalized cross-validation criterion or the empirical Bayes method (Farquharson and Oldenburg, 2004; Malinverno and Briggs, 2004; van den Berg and Friedlander, 2008; Hennenfent et al., 2008).

In this numerical example we estimate μ using the discrepancy principle and the L-curve. This formulation is preferred when an estimation of the noise level is available. To this end, we construct the L-curve of the data, also known as Pareto curve (van den Berg and Friedlander, 2008; Hennenfent et al., 2008), by carrying out the inversion using various trial μ values and plotting the resulting TV(X) versus misfit. Then, we choose the optimum μ as the one that minimizes the TV while the misfit remains less or equal than the noise level. Fig. 2 shows the Pareto curve corresponding to the inversion of the noisy seismic section shown in Fig. 1c. The blue vertical line indicates the TV associated with the actual AI image shown in Fig. 1a, the red horizontal line the noise level, and the black arrow the direction of increasing μ. As expected, the larger the μ, the smaller the TV and the larger the misfit, and vice versa. Following the discrepancy principle, we estimated the optimum value μ = 0.05 (yellow circle).

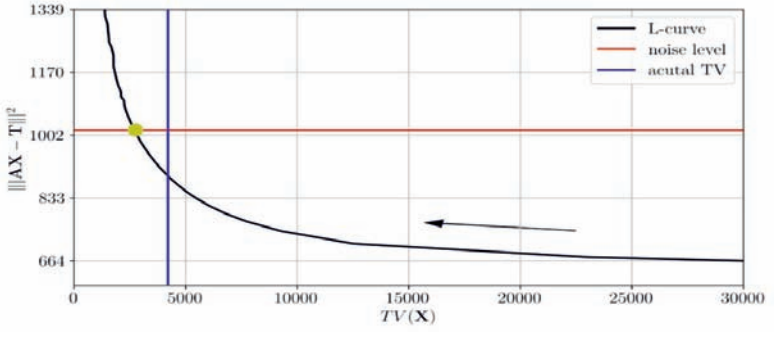

Fig. 2. Pareto curve after the inversion of the noisy data shown in Fig. 1d using Algorithm 1, for various trial values of μ. See text for details.

It is worth noting that the L-curve does not cross the intersection of the noise level and the actual TV of the AI, which would be the optimal solution of the problem. This behavior is expected because, as it is well-known, the TV regularization tends to underestimate the amplitudes of the estimated solutions (Paragios et al., 2005). Several authors have developed strategies to improve the amplitudes, such as the L^1 fitting (Nikolova, 2002) or the iterative refinement (Osher et al., 2005). Also, the use of a debiasing step to adjust the amplitudes after the iterative process was proposed in the context of other regularized inversion problems (Figueiredo et al., 2007; Pérez et al., 2013). In this work, as the underestimation of the amplitudes resulted to be small, we choose not to apply any correction in benefit of the efficiency of the method.

For comparison purposes, we also solve the inverse problem using the l_2- and l_1-norms as regularization terms. The corresponding cost functions become, respectively:

$$J(\mathbf{X}) = \frac{1}{\sigma^2}\|\mathbf{AX} - \mathbf{S}\|_2 + \lambda\|\mathbf{X} - \mathbf{T}\|_2 \quad , \tag{5}$$

and

$$J(\mathbf{X}) = \frac{1}{\sigma^2}\|\mathbf{AX} - \mathbf{S}\|_2 + \lambda\|\mathbf{X} - \mathbf{T}\|_2 + \mu\|\mathbf{DX}\|_1 \quad . \tag{6}$$

Eq. (5) corresponds to the classic Tikhonov regularization problem (Tikhonov and Arsenin, 1977), which leads to the least-squares solution. The second terms in the above two equations allow us to properly recover the low frequency trend and its impact is controlled by the trade-off parameter λ. In both cases we estimate λ via the discrepancy principle and the L-curve. The third term in eq. (6) is used to promote blocky solutions, as in the case of the TV semi-norm regularization. However, in the l_1-norm case, no constraints regarding the lateral continuity of the solution are involved, a fact that will become evident in the following example. We minimize eq. (6) using FISTA (Beck and Teboulle, 2009b).

Fig. 3 shows the results of the inversion of the data depicted in Fig. 1d for the three types of regularization. The first, second, and third rows of Fig. 3 show, respectively, the estimated impedances and data obtained using the l_2-norm, l_1-norm and TV regularizations. We observe that, in spite of honoring the observed data quite well, the three estimated AI images show different characteristics. As expected, the solutions obtained using the l_2-norm regularization (Fig. 3a) is much less blocky than its counterparts. Clearly, and because blockiness is not promoted, the low resolution of the resulting AI image hampers the interpretation of the results, as it is difficult to resolve thinner structures. Moreover, we observe some high-frequency instabilities in the estimated amplitudes. We could have minimized this

undesired effect by increasing the trade-off parameter λ, but at the expense of decreasing the resolution even more. The l_1-norm regularized solution (Fig. 3c), on the contrary, exhibits a structure that resembles the actual model more accurately, but shows a lack of lateral continuity because no lateral constraints are imposed during the inversion process. On the other hand, we observe that the TV solution is capable of estimating a consistent and sharp AI image (Fig. 3e) that clearly resembles the actual AI image shown in Fig. 1a. In contrast to the l_1-norm solution, the TV AI image shows good lateral continuity, preserving both major geological structures and detail features such as thin beds, faults and other minor structures that were almost hidden by the noise present in the data.

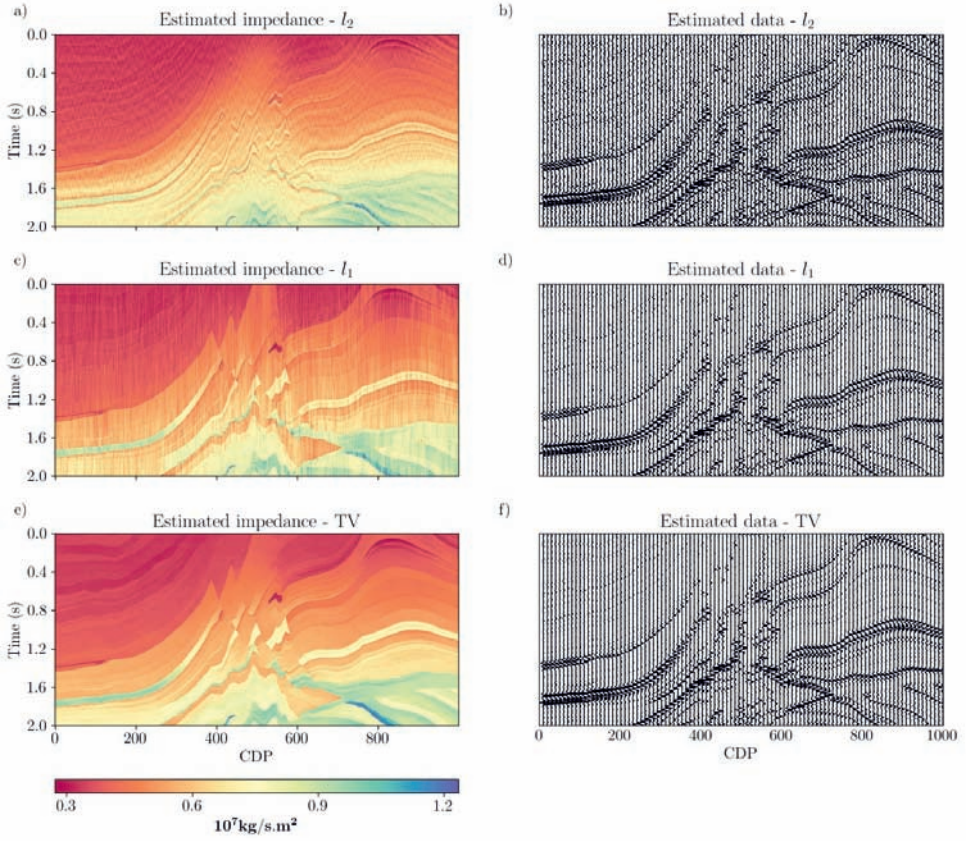

Fig. 3. Estimated AI from the seismic data shown in Fig. 1d using a) l_2-norm regularization, c) l_1-norm regularization and e) TV regularization. Estimated data from the b) l_2- norm solution, d) l_1-norm solution and f) TV solution.

Field data example

In this section we test the method using field data. Field data complicates the application of the method because not only the noise level is unknown, but also the source wavelet is often not available. We assume that the data has been properly processed to preserve amplitudes. The wavelet used in the inversion was estimated from the seismic section using the technique proposed by Gelpi et al. (2017). The low-frequency trend was estimated using well log data near to the area where the data was acquired. In this example we estimate the trade-off parameters by trial and error. The field dataset, shown in Fig. 4, consists of 260 traces with a sampling interval of 2 ms. The inversion was carried out in a time window of 1.0 s.

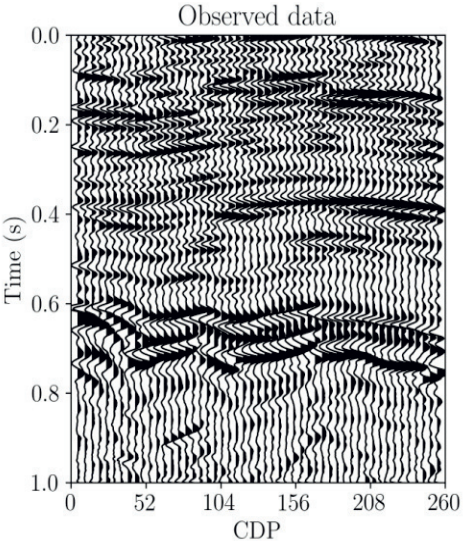

Fig. 4. Field data used to test Algorithm 1.

The first row of Fig. 5 shows the estimated solutions using the l_2-norm, the l_1-norm and the TV. As in the synthetic data example, the solutions obtained using the l_2-norm regularization (Fig. 5a) is less blocky than the others. The solution estimated using the l_1-norm (Fig. 5b) exhibits more blockiness, but with some lateral continuity issues. Finally, the solution estimated using the TV (Fig. 5c) overcomes the previous limitations, showing both well-defined blockiness and good lateral continuity. The second row of Fig. 5 shows the reconstructed data for each case, where we observe that the estimated solutions honor the observations very well in all cases.

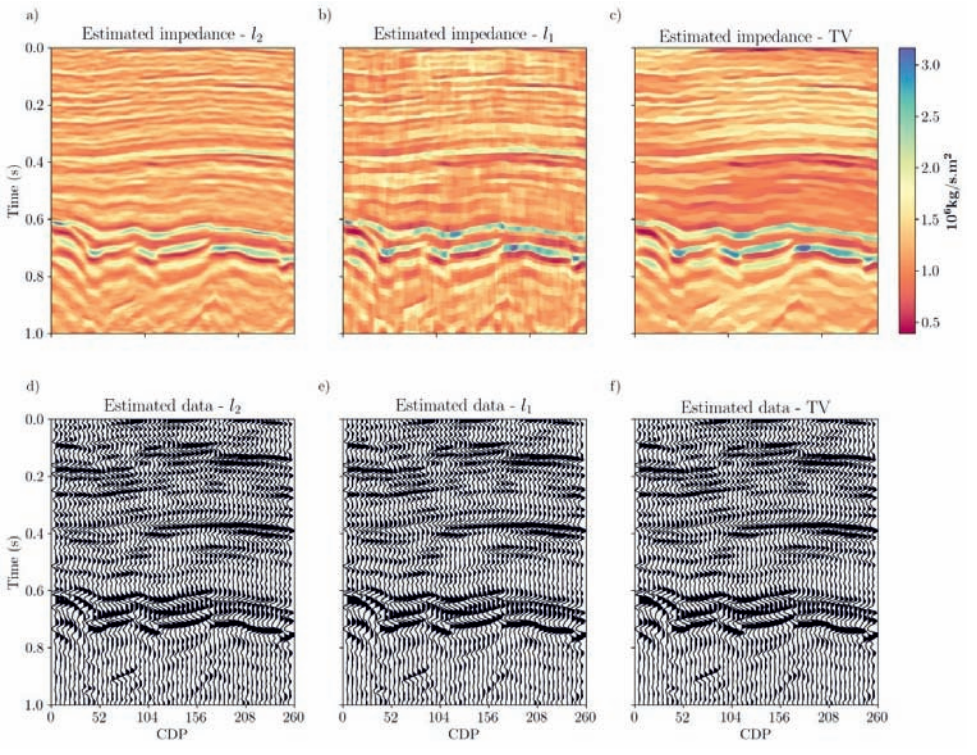

Fig. 5. Estimated AI from the seismic data shown in Fig. 4 using a) l_2-norm regularization, b) l_1-norm regularization and c) TV regularization. Estimated data from the d) l_2- norm solution, e) l_1-norm solution and f) TV solution.

CONCLUSIONS

In this work we presented a multichannel inversion algorithm to estimate sharp images of the acoustic impedance from poststack seismic data. When dealing with noisy and band-limited data, and due to the ill-posed nature of inverse problems, an appropriate regularization is needed to obtain meaningful solutions. To this end, we advocate the use of the total variation semi-norm, an adequate choice because it allows to handle edges properly. Because both the misfit between the calculated and observed data and the total variation semi-norm are convex function, the resulting cost function is convex and easily minimized using a gradient-based algorithm. In addition, since the proposed algorithm relies only on matrix-vector multiplications, the inversion method was computationally efficient and numerically stable. Contrarily to other TV-based methods described in the literature, the strategy that we propose is very versatile, simple, and efficient. One advantage is that it allows to easily incorporate the low frequency trend

without the need to include an additional trade-off parameter. Thus, the proposed method depends, as opposed to other methods published in the literature, on a single trade-off parameter, which can be easily tuned by trial-and-error. We tested the algorithm on 2D synthetic and field data and compared the results against the l_2- and l_1-norm solutions. We demonstrated that the TV algorithm is capable of obtaining sharp AI images that honor the observed data. In contrast to the l_2- and l_1-norm solutions, the TV AI images show good lateral continuity and properly estimated amplitudes, preserving the low frequency trend and overcoming their limitations.

ACKNOWLEDGMENTS

This work was partially supported by Programa de Incentivos, Universidad Nacional de La Plata (UNLP), Consejo Nacional de Investigaciones Científicas y Técnicas (CONICET, PIP 112-201201-00626-CO), and YPF Tecnología S.A.

REFERENCES

Beck, A. and Teboulle, M., 2009a. Fast gradient-based algorithms for constrained total variation image denoising and deblurring problems. IEEE Transact. Image Process., 18: 2419-2434.

Beck, A. and Teboulle, M., 2009b. A fast iterative shrinkage-thresholding algorithm for linear inverse problems. SIAM J. Imag. Sci., 2: 183-202.

Chambolle, A., 2004. An algorithm for total variation minimization and applications. J. Mathemat. Imag. Vis., 20: 89-97.

Cooke, D. and Schneider, W., 1983. Generalized linear inversion of reflection seismic data. Geopphysics, 46: 665-676.

Farquharson, C.G. and Oldenburg, D.W., 2004. A comparison of automatic techniques for estimating the regularization parameter in non-linear inverse problems. Geophys. J. Internat., 156: 411-425.

Figueiredo, M.A.T., Nowak, R.D. and Wright, S.J., 2007. Gradient projection for sparse reconstruction: Application to compressed sensing and other inverse problems. IEEE J. Select. Top. Sign. Process., 1: 586-597.

Gelpi, G.R., Pérez, D.O. and Velis, D.R., 2017. Estimación de la fase de la ondícula sísmica mediante la minimización de la norma l_1. XVII Worksh. Informat. Process. Contr. (RPIC): 1-6.

Gholami, A., 2015. Nonlinear multichannel impedance inversion by total-variation regularization. Geophysics, 80: R217-R224.

Gholami, A., 2016. A fast automatic multichannel blind seismic inversion for high-resolution impedance recovery. Geophysics, 81: V357-V364.

Gholami, A. and Sacchi, M.D., 2013. Fast 3D blind seismic deconvolution via constrained total variation and gcv. SIAM J. Imag. Sci., 6: 2350-2369.

Goldstein, T. and Osher, S., 2009. The split Bregman method for l_1-regularized problems. SIAM J. Imag. Sci., 2: 323-343.

Gramfort, A., Strohmeier, D., Haueisen, J., Hämäläinen, M. and Kowalski, M., 2013. Time-frequency mixed-norm estimates: Sparse m/eeg imaging with non-stationary source activations. NeuroImage, 70: 410-422.

Hennenfent, G., van den Berg, E., Friedlander, M.P. and Hermann, F.J., 2008. New insights into one-norm solvers from the Pareto curve. Geophysics, 73: 23-26.

Larson, R. and Edwards, B.H., 1999. Elementary Linear Algebra, 4th ed.. Houghton Mifflin Company, Boston.

Li, S. and Peng, Z., 2017. Seismic acoustic impedance inversion with multi-parameter regularization. J. Geophys. Engineer., 14: 520.

Liu, X. and Yin, X., 2015. Blocky inversion with total variation regularization and bounds constraint. Expanded Abstr., 85th Ann. Internat. SEG Mtg., New Orleans: 3497-3501.

Malinverno, A. and Briggs, V.A., 2004. Expanded uncertainty quantification in inverse problems: Hierarchical bayes and empirical bayes. Geophysics, 69: 1005-1016.

Martin, G.S., Wiley, R. and Marfurt, K.J., 2006. Marmousi2: An elastic upgrade for Marmousi. The Leading Edge, 25: 156-166.

Nikolova, M., 2002. Minimizers of cost-functions involving nonsmooth data-fidelity terms. Application to the processing of outliers. SIAM J. Numer. Analys., 40: 965-994.

Oldenburg, D.W., Scheuer, T. and Levy, S., 1983. Recovery of the acoustic impedance from reflection seismograms. Geophysics, 48: 1318-1337.

Osher, S., Burger, M., Goldfarb, D., Xu, J. and Yin, W., 2005. An iterative regularization method for total variation-based image restoration. Multisc. Model. Simulat., 4: 460-489.

Palomar, D.P. and Eldar, Y.C. (Eds.), 2010. Convex Optimization in Signal Processing and Communications. Cambridge University Press, Cambridge.

Paragios, N., Chen, Y. and Faugeras, O., 2005. Handbook of Mathematical Models in Computer Vision. Springer USA, New York.

Pérez, D.O., Velis, D.R. and Sacchi, M.D., 2013. High-resolution prestack seismic inversion using a hybrid FISTA least-squares strategy. Geophysics, 78: R185-R195.

Rudin, L.A., 1987. Images, Numerical Analysis of Singularities and Shock Filters. PhD thesis, California Institute of Technology, Pasadena.

Rudin, L.I., Osher, S. and Fatemi, E., 1992. Nonlinear total variation based noise removal algorithms. Physica D: Nonlin. Phenom., 60: 259-268.

Tarantola, A., 2005. Inverse problem theory and methods for model parameter estimation: SIAM J. Appl. Mathemat.

Tikhonov, A. and Arsenin, V., 1977. Solutions of Ill-posed Problems. Scripta Series in Mathematics. V.H. Winston, Maryland.

Ulrych, T.J. and Sacchi, M.D., 2005. Information-based Inversion and Processing with Applications. Elsevier Science Publishers, Amsterdam.

van den Berg, E. and Friedlander, M., 2008. Probing the Pareto frontier for basis pursuit solutions. SIAM J. Sci. Comput., 31: 890-912.

Velis, D.R., 2003. Estimating the distribution of primary reflection coefficients. Geophysics, 68: 1417-1422.

Velis, D.R., 2005. Constrained inversion of reflection data using Gibbs' sampling. J. Seismic Explor., 14,: 31-49.

Velis, D.R., 2008. Stochastic sparse-spike deconvolution. Geophysics, 73: R1-R9.

Walden, A. and J. Hosken, J., 1986. The nature of the non-Gaussianity of primary reflection coefficients and its significance for deconvolution. Geophys. Prosp., 34: 1038-1066.

Wang, D. and Gao, J., 2017. Multichannel seismic impedance inversion with anisotropic total variation regularization. Internat. Geophys. Conf., Qingdao, China, 17-20 April: 500-504.

Wang, Y., Cheng, S., She, B., Li, W., Hu, G., Liu, W. and Wang, X., 2017. Sharp laterally constrained multitrace impedance inversion based on blocky coordinate descent. Expanded Abstr., 87th Ann. Internat. SEG Mtg., Houston: 667-671.